stroke remains a major cause of morbidity and mortality in the US and globally. Less than a third of AIS patients are eligible for intervention and among successfully recanalized patients, more than half of patients do not achieve functional independence. Post-ischemic neuroinflammation remains a major contributor to secondary injury and worsening of outcomes after ischemic stroke by promoting loss of otherwise salvageable brain tissue. In this work, we designed a fusion protein (Psel-Crry) that binds to P-selectin, a protein expressed on inflamed endothelium and promotes platelet adhesion, and Crry which inhibits activation of the inflammatory system by targeting complement activation.

Hypothesis Following transient middle cerebral artery occlusion (MCAO) in mice, Psel-Crry homes specifically to the ischemic brain preventing complement activity and platelet aggregation leading to improved neurological outcome.

Methods The fusion protein Psel-Crry was constructed by linking the single-chain variable fragment (scFv) of anti-Pselectin antibody and the extracellular region of mouse Crry using overlapping PCR with the inclusion of a $(G_4S_2)_2$ linker sequence. The fusion was cloned into Expi293 cell, and purified using His60 Nickel column prior to concentration for intravenous injection. In-vitro complement inhibitory activity and Pselectin binding was assessed. Stroke was induced in 8-week-old C57bl6/j mice using the transient MCAO model by placing an intraluminal filament through the internal carotid artery ending at the MCA origin for 60 min followed by withdrawal of filament and reperfusion. In-vivo targeting was assessed using in-vivo fluorescent tomography. Neurological deficit was assessed over 3 days using the Neurological Severity Scale in mice, and infarct volume was computed from Nissl Stain.

Results Using surface plasmon resonance, Psel-Crry retained the ability to bind to Pselectin with moderate binding affinity, and demonstrated dose-dependent suppression of complement activity. Using in-vivo fluorescent tomography, administration of labeled Psel-Crry was found to specifically localize to the ipsilateral hemisphere when administered 2 h after MCAO and was retained at the site for at least 72 hours. Compared with vehicle (N=8), mice treated with Psel-Crry (N=10) showed significant reduction in C3 activation (40% reduction, $p<0.05$), overall cerebral edema (55% reduction, $p<0.01$), and infarct volume ($p<0.05$) 3 days after stroke. Psel-Crry significantly improved neurological deficit scores at 24 and 72 h after stroke ($p<0.05$). Mortality rate within 72 hrs was 70% in Psel-Crry compared to 40% in vehicle controls.

Conclusion Psel-Crry is a novel approach to target both platelet aggregation and complement-mediated neuroinflammation after stroke resulting in improved neurological outcomes in murine MCAO. Further preclinical characterization of chronic outcomes is ongoing in anticipation for clinical development.

Disclosures A. Alawieh: 1; C; Department of VA. 6; C; US Patent App. 17/335,355. **S. Tomlinson:** 1; C; Department of VA, NIH/NINDS. 4; C; Q3 Bio. 6; C; US Patent App. 17/335,355.

O-029 TARGETING MICROGLIA FOR CEREBRAL VASOSPASM FOLLOWING SUBARACHNOID HEMORRHAGE

B Lucke-Wold*. *Neurosurgery, University of Florida, Gainesville, FL*

10.1136/neurintsurg-2022-SNIS.29

Background Cerebral vasospasm (CV) can contribute significant morbidity for subarachnoid hemorrhage (SAH) patients. A key unknown is how CV induction is triggered following SAH.

Methods c57/bl6 wild type and c57/bl6 dual reporter mice were utilized: saline injected, SAH, SAH + microglia inhibited mice were used. For SAH, 50 mm blood was collected from tail puncture and administered into basal cisterns. Microglia inhibition was induced 3 days prior to SAH via pharmaceutical means. Confirmed >70% reduction in microglia was verified. Various markers of neuroinflammation were measured with western blot and immunohistochemistry. Cerebral blood flow was measured to look at spreading cortical depolarizations. Vasospasm was measured via cardiac injection of india-ink/gelatin. Turning test and Garcia's modified SAH score were utilized. $P<0.05$ was considered significant.

Results Dual reporter mice showed peripheral macrophages and microglia aggregation near basal cisterns indicating significant cross talk. Ferritin uptake by microglia was significant in perivascular and periventricular distribution. A significant increase in BBB markers ZO-1 and occludin were noted following SAH but reduced with microglia depletion ($p<0.05$). CV occurred 5 days post SAH but was reduced in microglia depleted mice ($p<0.05$). SAH mice had impaired performance on turn test and poor Modified Garcia Scores compared to saline. A distinct microglia phenotype was noted day 5 in the SAH group (overlap coefficients r=0.96 and r=0.94) for Arg1 and iNOS, but this was drastically altered by microglia depletion. Microglia depletion limited the ferritin uptake, which has been shown to be a triggering event for vasospasm. Peripheral macrophage clearance was seen starting day 9 in the dual reporter mice. Prior to this point, peripheral macrophages had undergone diapedesis into parenchyma likely inciting the vasopsasm response. Increases in NFkappaB and NADPH oxidase pathways were seen following SAH at day 9 ($p<0.05$)

Conclusion Microglia activation is critical for CV and we show that this process is mediated by ferritin uptake and crosstalk with peripheral macrophages. Long term neuroinflammatory cascades were initiated. These novel findings show a potential therapeutic target that previously has not been readily investigated.

Disclosures B. Lucke-Wold: None.

O-030 HISTOLOGICAL ANALYSIS OF THE DURA-MEMBRANE INTERFACE OF CHRONIC SUBDURAL HEMATOMAS

[1]M Potts*, [2]M Bitar, [1]A Alwakeal, [1]P Nazari, [1]B Jahromi. *[1]Neurological Surgery, Northwestern University Feinberg School of Medicine, Chicago, IL; [2]Pathology, Northwestern University Feinberg School of Medicine, Chicago, IL*

10.1136/neurintsurg-2022-SNIS.30

Introduction The vascular membrane that forms around chronic subdural hematomas (cSDHs) has been implicated in the development and persistence of these lesions. However, the pathology underlying the formation of this membrane is poorly understood. There is mounting evidence that middle meningeal artery embolization (MMAE) can successfully cure cSDHs by occluding the meningeal arteries overlying the cSDH membrane, but the exact mechanism of this treatment is also poorly understood. We therefore sought to perform a histopathological characterization of the interface between the dura and cSDH membrane to begin to elucidate the

underlying pathology of cSDH membranes and mechanism of MMAE.

Methods We retrospectively reviewed the clinical history and histology of 13 patients with cSDH who underwent surgical evacuation and resection of the dura with attached cSDH membrane. Specimens were formalin-fixed and paraffin-embedded. Standard H&E-stained sections were obtained for all cases and submitted for routine pathological evaluation. Brain autopsy dura samples from non-cSDH cases were used as controls.

Results All patients presented with symptomatic cSDH. The mean age was 76.8 years and nine patients were male. Seven patients had a definite history of a prior remote fall or head trauma preceding diagnosis of the cSDH ranging from two to 12 weeks. Two patients presented with bilateral cSDHs. Histological analysis of the dura-membrane interface in all cases revealed cSDH membranes consisting of exuberant organizing chronic hematoma with fibroblasts, small blood vessels, chronic inflammation, and hemosiderin deposits. Fresh hemorrhage was often found just beneath the cSDH membrane. Variable and focally pronounced vascular proliferation of small blood vessels was evident along the dura-membrane interface. Immunohistochemical analysis in select cases confirmed the presence of pronounced vascular proliferation including endothelial cells (+nuclear ERG staining) and vascular wall smooth muscle cells (+cytoplasmic SMA staining) along the dura-membrane interface. Such proliferation was not seen in normal control dura samples in brain autopsy material.

Conclusions The dural interface with a cSDH membrane is characterized by abnormal vascular proliferation. Such proliferation may be involved in the formation of the cSDH membrane and may play a role in the underlying mechanism of MMAE. Further investigation is warranted.

Disclosures M. Potts: None. **M. Bitar:** None. **A. Alwakeal:** None. **P. Nazari:** None. **B. Jahromi:** None.

O-031 CATHETER TIP SHAPE OPTIMIZATION USING A PARAMETERIZED MODEL OF THE SIMMONS CATHETER

[1]K Zerebiec, [2]J Boyle, [3]L Silveira, [3]J Muse, [4]G Kreuser, [5]T Paris, [6]R Floreani, [2]D Johnson, [2]S Raymond*. *[1]Neurology, The University of Vermont Medical Center, Burlington, VT; [2]Radiology, The University of Vermont Medical Center, Burlington, VT; [3]Neurosurgery, The University of Vermont Medical Center, Burlington, VT; [4]Biomedical Engineering, The University of Vermont, Burlington, VT; [5]Mechanical Engineering, The University of Vermont, Burlington, VT; [6]Mechanical and Biomedical Engineering, The University of Vermont, Burlington, VT*

10.1136/neurintsurg-2022-SNIS.31

Introduction/Purpose Many practitioners have transitioned from transfemoral to a radial first approach for cerebral angiography due to the improved safety profile and patient satisfaction. The Simmons 2 catheter is the most commonly used and is adequate but not optimized for transradial cerebral angiography. In this study, we built a library of reverse curve catheter shapes based on variations in the Simmons 2 design and tested library performance in a silicone transradial aortic arch model.

Materials and Methods The reverse curve shape is defined by 9 parameters that describe three curves and adjacent segments (figure 1): the three angles (A1–3), the radius of curvature at each of the angles (R1–3) and the segment lengths (D1–3). For the classic Simmons 2 shape, A1 is 180 degrees, A2 is 15 degrees and A3 is approximately 245 degrees. We designed shaping forms with varying A1 (180, 210, and 240 degrees, figure 2) using the parameterized model in Onshape, a browser-based computer aided design platform, to draw plates with 5 Fr width grooves following the desired catheter tip shape. These shaping forms were then produced in aluminum by CNC-milling (Xometry). The straight 5 Fr Terumo GLIDECATH was used as a stock catheter and shaped by heating the catheter in the form at 160 degrees Celsius for 15 minutes with immediate quenching in room temperature water. Catheter performance was evaluated with two tasks: catheter reforming at the arch (without a wire) and great vessel selection from the arch using a silicone transradial aortic arch model (Mentice). Three trainee operators performed 10 timed trials of each task with each catheter.

Results Catheter reformation at the arch was slightly faster for the 210 degree catheter but similar to slightly slower for the 240 degree catheter. Vessel selection was similar for all of the catheters with some variation between operators.

Conclusions Catheter tip shape affects performance of maneuvers including tip reformation at the arch and vessel selection. We demonstrated an approach for rapid tip shape prototyping and performance evaluation in a silicone arch model and used

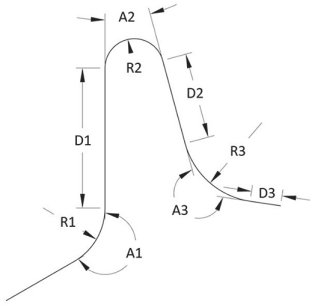

Figure 1. Parametric model of the reverse curve catheter shape. The reverse curve is composed of three turns and adjacent segments, defined by the three angles, A1-3, and associated radii of curvature, R1-3, and adjacent segments, D1-3. The classic Simmons 2 shape has A1 = 180 degrees (no turn), A2 = 15 degrees, and A3 approximately 245 degrees.

Abstract O-031 Figure 1 Parametric model of the reverse curve catheter shape. The reverse curve is composed of three turns and adjacent segments, defined by the three angles, Al-3, and associated radii of curvature, R1–3, and adjacent segments, D1–3. The classic Simmons 2 shape has A1 = 180 degrees (no turn), A2 = 15 degrees, and A3 approximately 245 degrees

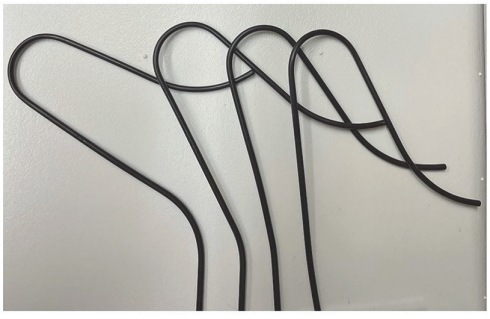

Figure 2. Reverse curve catheters with varying A1. Catheters with increasing A1 from right to left of 180, 195, 210 and 240 degrees.

Abstract O-031 Figure 2 Reverse curve catheters with varying A1. Catheters with increasing A1 from right to left of 180, 195, 210 and 240 degrees